In-Plane Transport and Enhanced Thermoelectric Performance in Thin Films of the Topological Insulators Bi_2Te_3 and Bi_2Se_3

Pouyan Ghaemi,[1,2] Roger S. K. Mong,[1] and J. E. Moore[1,2]

[1]*Department of Physics, University of California at Berkeley, Berkeley, California 94720, USA*

[2]*Materials Sciences Division, Lawrence Berkeley National Laboratory, Berkeley, California 94720, USA*

(Received 31 March 2010; published 11 October 2010)

Several small-band-gap semiconductors are now known to protect metallic surface states as a consequence of the topology of the bulk electron wave functions. The known "topological insulators" with this behavior include the important thermoelectric materials Bi_2Te_3 and Bi_2Se_3, whose surfaces are observed in photoemission experiments to have an unusual electronic structure with a single Dirac cone. We study in-plane (i.e., horizontal) transport in thin films made of these materials. The surface states from top and bottom surfaces hybridize, and conventional diffusive transport predicts that the tunable hybridization-induced band gap leads to increased thermoelectric performance at low temperatures. Beyond simple diffusive transport, the conductivity shows a crossover from the spin-orbit-induced antilocalization at a single surface to ordinary localization.

DOI: 10.1103/PhysRevLett.105.166603 PACS numbers: 72.20.Pa, 03.65.Vf, 72.25.−b, 73.50.Lw

Manipulation of phonon thermal conductivity [1,2] and electronic structure by quantum confinement [3] have both been active areas of thermoelectric research, but the recent discovery that some of the best thermoelectrics are three-dimensional "topological insulators" (TIs) [4–8] suggests new directions for this field. For straightforward reasons, similar materials are required for TI behavior and for high thermoelectric figure of merit (zT) $zT = \frac{S^2\sigma T}{\kappa}$, where S is the thermopower (Seebeck) coefficient, σ is the electrical conductivity, and κ is the thermal conductivity. TIs require heavy elements in order to generate large spin-orbit coupling, which drives the formation of the topological surface state, and a small band gap so that the spin-orbit coupling can modify the band structure by "inverting" one band.

Similarly, thermoelectric semiconductors typically consist of heavy elements in order to obtain low phonon thermal conductivity and have a small band gap (of the order of 5–10 times k_BT, where T is the operating temperature) in order to obtain a large electronic power factor σS^2. An example is Bi_2Te_3, which has one of the highest known bulk thermopower figures of merit [9] and for decades has been used for thermoelectric devices [10].

Many approaches have already been tried to improve thermoelectric performance of Bi_2Te_3, e.g., tuning carrier concentration (to increase S), decreasing the thermal conductivity through alloying [11,12], inducing crystal defects or nanostructures [13], and making thin films to control transport of phonons and electrons [14]. Photoemission experiments reveal that Bi_2Te_3 is a TI with a single Dirac cone on the surface [5], consistent with electronic structure predictions [15]. Here we ask whether this new surface state could lead to improved thermoelectrics.

We start by deriving the effective surface Hamiltonian on symmetry grounds and then use the resulting band structure to compute the thermoelectric properties using standard diffusive transport. Because of the large bulk gap ($\Delta_{\text{gap}} \sim 165$ meV), the chemical potential could be tuned to be in the bulk band gap [5], and in this regime we can study the transport properties of the surface states independently. In closing, antilocalization effects in a thin film resulting from the spin-orbit-induced Berry phase are discussed.

The physical system to be studied here is a thin film of Bi_2Te_3. If the film is thin enough, the surface states on both sides hybridize and open a gap [16–18]. Although the film thickness required to open an observable gap ($\sim$ 1–10 nm) is small, it is accessible with current growth and mechanical exfoliation [19] techniques, and very recently the hybridization gap has been observed by *in situ* photoemission on thin films of Bi_2Se_3 [20].

We obtain the effective Hamiltonian of a thin film in the basis labeled by spin and the surface [top(u)/bottom(d)] at which they are localized. The general effective Hamiltonian takes the block form:

$$H(\mathbf{p}) = \begin{pmatrix} H_u & V_{du} \\ V_{ud} & H_d \end{pmatrix}. \tag{1}$$

H_u and H_d are Hermitian, while $(V_{du})^\dagger = V_{ud}$. The diagonal block terms H_u and H_d are the effective Hamiltonians in the semi-infinite slab. The off-diagonal terms V_{du} and V_{ud} describe the coupling of the two surfaces.

The parity (inversion) symmetry in the Bi_2Te_3 structure puts constraints on the form of the Hamiltonian in Eq. (1) that are strongest if the top and bottom surfaces are related by parity. Parity (Π) exchanges the top and bottom surfaces, changes the sign of the momenta $\mathbf{p}$, but has no effect on spin: $\Pi H(\mathbf{p})\Pi^{-1} = H(-\mathbf{p})$. Time reversal ($\mathcal{T}$) exchanges the spins and flip the momenta: $\mathcal{T}H(\mathbf{p})\mathcal{T}^{-1} = H(-\mathbf{p})$. Explicitly, $\Pi = \tau^x\sigma^0$ and $\mathcal{T} = -i\tau^0\sigma^y\mathcal{K}$, where τ's are Pauli matrices in the up (down) surface space and $\mathcal{K}$ is the complex conjugation operator.

The combination of parity and time reversal implies $\Pi\mathcal{T}H(\mathbf{p})(\Pi\mathcal{T})^{-1} = H(\mathbf{p})$, which gives $\sigma^y H_u^* \sigma^y = \sigma^y H_u^T \sigma^y = H_d$ and $\sigma^y V_{du}^T \sigma^y = V_{du}$. It is useful to note the identities $\sigma^y(\sigma^i)^T\sigma^y = -\sigma^i$ for $i = x, y, z$ and $\sigma^y I^T \sigma^y = I$. If we decompose the matrix $H_u = cI + \mathbf{a}\cdot\boldsymbol{\sigma}$, then $\sigma^y H_u^T \sigma^y$ flips the sign of the Pauli matrices components $\mathbf{a}\cdot\boldsymbol{\sigma}$ but leaves the identity component cI: $H_d = cI - \mathbf{a}\cdot\boldsymbol{\sigma}$. Since H_u is Hermitian, c is real and $\mathbf{a}$ is a real vector. For $V_{du} = \Delta_f I + \boldsymbol{\Delta}_f \cdot \boldsymbol{\sigma}$ the Pauli matrices components vanish so $V_{du} = \Delta_f I$, with complex Δ_f.

$$H(\mathbf{p}) = \begin{pmatrix} \mathbf{a}(\mathbf{p})\cdot\boldsymbol{\sigma} & \Delta_f(\mathbf{p}) \\ \Delta_f^*(\mathbf{p}) & -\mathbf{a}(\mathbf{p})\cdot\boldsymbol{\sigma} \end{pmatrix} + c(\mathbf{p}). \tag{2}$$

Without loss of generality, we can find a suitable gauge transformation such that Δ_f is real; this gauge transformation is allowed by the phase ambiguity in the parity operator between the top and bottom states.

By using parity to relate the parameters $\mathbf{a}$, Δ_f, and c at opposite momenta, there are further constraints: $\mathbf{a}(-\mathbf{p}) = -\mathbf{a}(\mathbf{p})$, $\Delta_f(-\mathbf{p}) = \Delta_f(\mathbf{p})^*$, and $c(-\mathbf{p}) = c(\mathbf{p})$. Near the Dirac cone, we expand the Hamiltonian to the first order in $\mathbf{p}$. As Δ_f and c are even in $\mathbf{p}$, they can be treated as constant, while $\mathbf{a}$ is odd in $\mathbf{p}$ and we keep only the linear term, of the form $V_D\mathbf{p}\cdot\boldsymbol{\sigma}$ for Bi_2Te_3 (isotropic velocity).

From *ab initio* calculations [15] one can find parameters for H and the dispersion of the surface modes $E_\mathbf{p} = \pm\sqrt{(V_D\mathbf{p})^2 + \Delta_f^2}$,

$$H(\mathbf{p}) = \begin{pmatrix} V_D\mathbf{p}\cdot\boldsymbol{\sigma} & \Delta_f \\ \Delta_f & -V_D\mathbf{p}\cdot\boldsymbol{\sigma} \end{pmatrix}, \tag{3}$$

$V_D \approx 4.05\times10^5$ m/s [5] (in thin films it is between 3.4×10^5 and 4.6×10^5 m/s [20]) indicates the Dirac velocity, and $\mathbf{p}$ is the momentum with respect to the Dirac point.

Now using the electron dispersion above we obtain the in-plane transport coefficients for the surface states [21]: $\sigma/e^2 = I_0$, $T\sigma S/e = I_1$, and $T\kappa_0 = I_2$, where

$$I_n = \int_{-\infty}^{\infty} d\varepsilon \frac{\partial f(\varepsilon)}{\partial\varepsilon}\Sigma(\varepsilon)(\varepsilon - E_f)^n. \tag{4}$$

σ is conductivity and S is the Seebeck coefficient. κ_0 is the electronic thermal conductivity at constant electrochemical potential, where for zero electric current $\kappa_e = \kappa_0 - S^2\sigma T$. $\Sigma(\varepsilon) = N(\varepsilon)\tau(\varepsilon)\nu_x(\varepsilon)^2$ is the conductivity density, and $f(\varepsilon)$ is the Fermi-Dirac distribution function. Experiments on bulk Bi_2Te_3 and its topologically protected surface states show the hybridization gap $\sim$25 meV [5,22], which is achievable with recently created nanometer thick films [16,17,20].

Below 150 K, zT from surface states (Fig. 1) is large compared with current low-temperature thermoelectric materials in a relatively large range of chemical potential (e.g., Na_xCoO_2 [23] and $CsBi_4Te_6$ [24]). In the thin film, transport properties of the surface states should be considered in parallel with the bulk of the thin film. Because of its

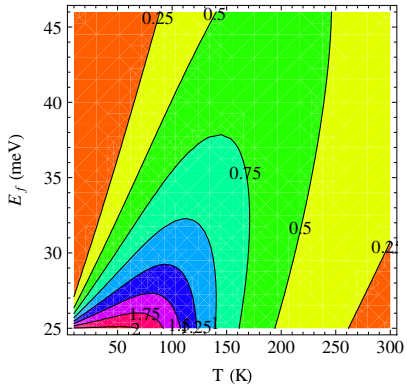

FIG. 1 (color online). zT of surface states alone as a function of chemical potential relative to the center of the surface gap and temperature.

thermoelectric performance ($zT \sim 0.6$) at room temperature, the bulk properties of Bi_2Te_3 have been widely studied [10,22]. The zT for the whole film is $zT = \frac{(S_f\sigma_f + S_b\sigma_b d)^2 T}{(\sigma_f+\sigma_b d)(\kappa_f+\kappa_b d)}$. f and b stand for surface and bulk properties, respectively, and d denotes the film thickness. Using the bulk properties [25,26] for the temperature range where surface states have high zT, we can estimate the total zT for the thin film (but note that using a single value for the bulk contribution at a given temperature, since the transport properties even in bulk depend strongly on the Fermi level). Figure 2 shows zT versus the Fermi level for $d =$ 1 nm thick films at 175, 150, 100, and 50 K.

Thermoelectricity from ballistic gapless 1D edge states in a 2D quantum spin Hall nanoribbon was discussed recently by Takahashi and Murakami [27]. Thin films of some 3D TIs are in quantum spin Hall states [17], so the edge states could contribute also in a narrow film. However, in the quantum spin Hall proposal the chemical potential is in the bulk bands; here it is in the gap.

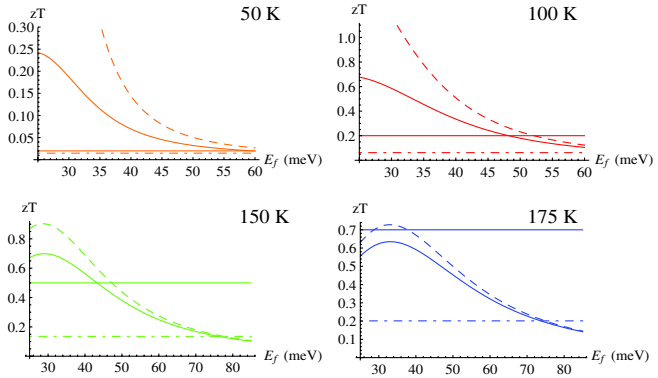

FIG. 2 (color online). zT (curved solid line) for the thin film including bulk contributions as a function of chemical potential. zT for $CsBi_4Te_6$ [24] (straight solid line), the surface states alone (dashed line), and bulk Bi_2Te_3 (dashed-dotted line). $\sigma_b \times 10^{-5}$ $(\Omega\mathrm{m})^{-1} = 2, 1.25, 0.83, 0.72$, $\kappa_b(\mathrm{W\,K^{-1}\,m^{-1}}) = 3.35, 2.83, 2.35, 2.2$, and $S_b \times 10^6$ $(\mathrm{V\,K^{-1}}) = 70, 115, 150, 171$ at $T = 50$, 100, 150, and 175 K, respectively [25,26].

At temperatures below 150 K, which are important for several Peltier cooling applications, the thermoelectric performance of the TI thin film is significantly enhanced (Fig. 2) because of the high zT of the protected edge states. At low temperature the bulk contribution is smaller than the surface contribution so that the unknown chemical potential dependence of bulk properties is not too significant. Crucially, the gap in the hybridized surface mode band structure can be controlled by tuning the thickness of the film to get high zT in a specific temperature range. The source of the improved thermoelectric properties is the power factor $S^2\sigma$: As a result of surface band structure, at the optimal chemical potential, which is a function of temperature, both S and σ are increased relative to those of the bulk material at optimal doping (see Fig. 3). The geometry of thin films is also very effective in reduction of phonon thermal conductivity [1,2,19], so there will be even larger enhancement for the TI thin films such as Bi_2Te_3, Bi_2Se_3, and $Bi_2Se_xTe_{3-x}$.

The conductivity$\sigma = e^2 I_0$ is calculated by using Boltzmann formalism [28], i.e., classical trajectories of electrons. Quantum mechanical corrections appear as the interference of quantum phases of different trajectories. In a simple picture, the amplitude for an electron moving between two positions (a and b) is given by $|\mathbf{A}_{ab}| = |\sum_n A_n e^{i\phi_n}|$, where n labels different classical paths between a and b and ϕ_n represents the corresponding quantum phase [29]. This phase is usually random and averages to zero (i.e., $|\mathbf{A}_{ab}|^2 = \sum_n |A_n|^2$), which leads to the Boltzmann conductivity. On the other hand, for closed trajectories where the electron returns to a region of size comparable to its quantum wavelength, quantum interference plays an important role. For diffusive motion, as in a metal, there is a finite probability for closed paths (Fig. 4). Such closed loops in ordinary metals lead to reduction of the conductivity (i.e., localization) [28]. Since such paths can be taken in two opposite directions, the relative phases do not average to zero; the corresponding quantum correction is $\frac{\delta\sigma}{\sigma} = -\cos(\phi^+ - \phi^-)$, where ϕ^+ and ϕ^- correspond to phases for two opposite trajectories.

Quantum corrections affect the conductivity of materials strongly at mesoscopic length scales [30]. Here we show that the chiral nature of states on the Fermi surface (FS) can increase the mean-free path even when hybridization

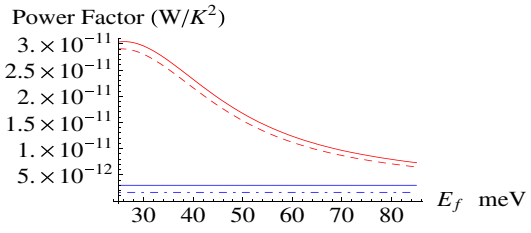

FIG. 3 (color online). Power factor ($S^2\sigma$) at 100 K: Thin film (solid red line), surface states (dashed red line), best known low-temperature thermoelectrics (solid blue line), and bulk Bi_2Te_3 (dotted-dashed blue line).

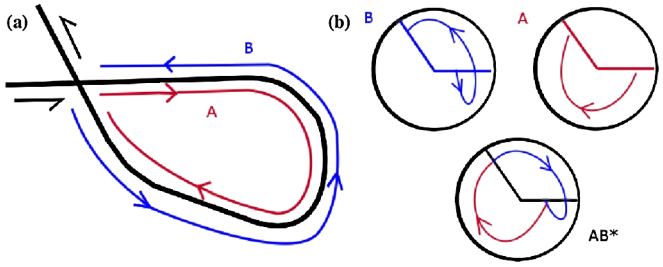

FIG. 4 (color online). Backscattering process: (a) Two trajectories (A and B) leading to backscattering in real space traveled in opposite directions. (b) A and B trajectories in momentum space. They add up to rotation of momentum by 2π.

is present. At each momentum, the effective surface Hamiltonian [Eq. (3)] has two degenerate eigenstates:

$$|a_{\mathbf{p}}\rangle = (0, \Delta_f, -pe^{-i\theta_{\mathbf{p}}}, E_{\mathbf{p}})^T/\sqrt{2}E_{\mathbf{p}},$$
$$|b_{\mathbf{p}}\rangle = (E_{\mathbf{p}}, pe^{i\theta_{\mathbf{p}}}, \Delta_f, 0)^T/\sqrt{2}E_{\mathbf{p}}, \quad (5)$$

where for simplicity $V_D = 1$ and $(p_x, p_y) = p(\cos\theta_{\mathbf{p}}, \sin\theta_{\mathbf{p}})$. On the FS p is fixed so states are labeled by $\theta_{\mathbf{p}}$'s. Although at each momentum $\mathbf{p}$ states $|a_{\mathbf{p}}\rangle$ and $|b_{\mathbf{p}}\rangle$ are orthonormal, they are not at different momenta:

$$2E_{\mathbf{p}}^2\langle a_{\mathbf{p}'} \mid a_{\mathbf{p}}\rangle = 2|\Delta_f|^2 + p^2[1 + e^{i(\theta_{\mathbf{p}'}-\theta_{\mathbf{p}})}],$$
$$2E_{\mathbf{p}}^2\langle b_{\mathbf{p}'} \mid b_{\mathbf{p}}\rangle = 2|\Delta_f|^2 + p^2[1 + e^{i(\theta_{\mathbf{p}}-\theta_{\mathbf{p}'})}], \quad (6)$$
$$2E_{\mathbf{p}}^2\langle a_{\mathbf{p}'} \mid b_{\mathbf{p}}\rangle = p\Delta_f(e^{i\theta_{\mathbf{p}}} - e^{i\theta_{\mathbf{p}'}}).$$

$\langle b_{\mathbf{p}} \mid a_{\mathbf{p}'}\rangle$ is small for small angle scatterings and small Δ_f. Any state of the form $|\psi_{\mathbf{p}}\rangle = \alpha|a_{\mathbf{p}}\rangle + \beta|b_{\mathbf{p}}\rangle$ is also an eigenstate with energy $E_{\mathbf{p}} = \sqrt{\Delta_f^2 + p^2}$.

Smooth impurities on the surface scatter different states on the FS into each other (i.e., they change $\theta_{\mathbf{p}}$) and lead to diffusive motion of quasiparticles and classical Boltzmann conductivity [28] $\sigma = \frac{ne^2\tau}{m}$, which we used. Quantum effects could be cast as the interference of quantum phases that quasiparticles gain while moving along different classical trajectories [29]. However, the phase differences between different trajectories are generally random and average to zero [28], with the exception of self-intersecting trajectories, which could be taken in two different directions. The relative phase is not random and leads to quantum interferences.

When $\Delta_f = 0$ (i.e., decoupled surfaces), clearly the state $|a_{\mathbf{p}}\rangle$ is affected only by impurities in the bottom surface and $|b_{\mathbf{p}}\rangle$ is affected by impurities in the top surface. In other words, a mixed state cannot go over a classical self-intersecting trajectory, since the direction of motion ($\theta_{\mathbf{p}}$) in $|a_{\mathbf{p}}\rangle$ and $|b_{\mathbf{p}}\rangle$ changes independently with scatterings in the bottom and top surfaces, so quantum interference effects are important only for pure $|a_{\mathbf{p}}\rangle$ and pure $|b_{\mathbf{p}}\rangle$ states.

When Δ_f is nonzero but small, $|a_{\mathbf{p}}\rangle$ and $|b_{\mathbf{p}}\rangle$ are mainly (but not entirely) localized in the bottom and top surfaces, and they depend only on the direction of momentum ($\theta_{\mathbf{p}}$)

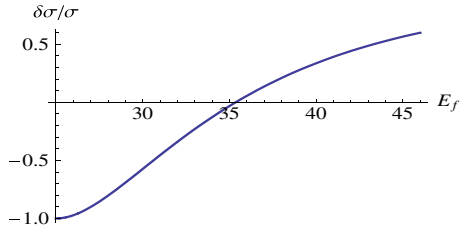

FIG. 5 (color online). Quantum corrections to the conductivity. Comparing with Fig. 2, we see a finite range over which antilocalization coexists with enhanced zT predicted from ordinary diffusive transport [Eq. (4)].

in the corresponding surfaces, respectively. As in the case with $\Delta_f = 0$, for randomly distributed impurities in the two surfaces, $|a_{\mathbf{p}}\rangle$ and $|b_{\mathbf{p}}\rangle$ can move over self-intersecting trajectories independently. However, in a mixed state, $|\psi_{\mathbf{p}}\rangle = \alpha|a_{\mathbf{p}}\rangle + \beta|b_{\mathbf{p}}\rangle$, the directions $\theta_{\mathbf{p}}$ change independently in two surfaces and do not simultaneously form closed loops (see Fig. 4). So to track the quantum interference effects we should consider $|a_{\mathbf{p}}\rangle$ and $|b_{\mathbf{p}}\rangle$ independently. The quantum phase of each trajectory is given by the associated Berry phase [31]: $\phi = -i\int_0^T dt\langle\Psi_{\mathbf{p}_t}|\frac{\partial}{\partial t}|\Psi_{\mathbf{p}_t}\rangle = \mp\frac{p^2}{2E_{\mathbf{p}}^2}(\theta_{\mathbf{p}_T} - \theta_{\mathbf{p}_0})$ for $\Psi = |a\rangle$ and $|b\rangle$, respectively.

The quantum amplitude of the closed trajectory corresponds to the sum of the of amplitudes when the self-intersecting path is taken in opposite directions; i.e., $|(e^{i\phi_1} + e^{i\phi_2})/\sqrt{2}|^2 = 1 + \cos(\phi_1 - \phi_2)$, where ϕ_1 and ϕ_2 correspond to the Berry phase passing over the closed loop in opposite directions. As can be seen in Fig. 4, $(\phi_1 - \phi_2)$ corresponds to the phase associated with rotation of θ_p by 2π. The corresponding Berry phase could be calculated: $\phi_1 - \phi_2 = \int_{\theta_0}^{\theta_0+2\pi} dt\langle\Psi(\mathbf{p}_t)|\frac{\partial}{\partial t}|\Psi(\mathbf{p}_t)\rangle = \pm\frac{p^2}{p^2+\Delta_f^2}\pi = \pm\frac{E_{\mathbf{p}}^2-\Delta_f^2}{E_{\mathbf{p}}^2}\pi$ for $\Psi = |a\rangle$ or $|b\rangle$. The two limits $p \to 0$ $(\Delta\phi \to 0)$ and $p \gg \Delta_f/V_D$ $(\Delta\phi \to \pm\pi)$ lead to localization and antilocalization behavior, respectively. With increasing the chemical potential, localization behavior changes into antilocalization, which is expected for a single TI surface. Comparing Fig. 5 with the Seebeck results in Fig. 1, we see that, in some range of chemical potential where the films have high thermoelectric performance, the antilocalization effect is also present. This leads to another advantage of the TI thin films: The quantum corrections increase the conductivity.

We found that simply creating a nanometer-scale thin film of Bi_2Te_3 generates a hybridization-induced band gap of the unconventional surface states that can be tuned by film thickness. This is indeed an essential feature for controlling the figure of merit in a material which is already thermoelectric in the bulk. Combined with some residual robustness against impurity scattering, this leads to an increased low-temperature zT of the film. The same technique can equally well be applied to Bi_2Se_3 or alloys in this class. While we have concentrated on the specific case of a thin film (or single superlattice layer) in this Letter, the topological surface state of these materials is an important physical feature that will also affect thermoelectric transport in other nanoscale geometries.

The authors acknowledge conversations with K. Hippalgaonkar and R. Ramesh and support from BES DMSE (P. G. and J. E. M.).

[1] A. Balandin and K. L. Wang, Phys. Rev. B **58**, 1544 (1998).
[2] A. Balandin and K. L. Wang, J. Appl. Phys. **84**, 6149 (1998).
[3] L. D. Hicks and M. S. Dresselhaus, Phys. Rev. B **47**, 12 727 (1993).
[4] Y. Xia *et al.*, Nature Phys. **5**, 398 (2009).
[5] Y. L. Chen *et al.*, Science **325**, 178 (2009).
[6] L. Fu, K. L. Kane, and E. J. Mele, Phys. Rev. Lett. **98**, 106803 (2007).
[7] J. E. Moore and L. Balents, Phys. Rev. B **75**, 121306(R) (2007).
[8] D. Hsieh *et al.*, Nature (London) **452**, 970 (2008).
[9] G. J. Snyder and E. S. Toberer, Nature Mater. **7**, 105 (2008).
[10] H. J. Goldsmid and R. W. Douglas, Br. J. Appl. Phys. **5**, 386 (1954).
[11] R. R. Heikes and R. W. Ure, *Thermoelectricity: Science and Engineering* (Interscience, New York, 1961).
[12] T. M. Tritt, Science **283**, 804 (1999).
[13] B. Poudel *et al.*, Science **320**, 634 (2008).
[14] R. Venkatasubramanian *et al.*, Nature (London) **413**, 597 (2001).
[15] H. Zhang *et al.*, Nature Phys. **5**, 438 (2009).
[16] J. Linder, T. Yokoyama, and A. Sudbo, Phys. Rev. B **80**, 205401 (2009).
[17] C.-X. Liu *et al.*, Phys. Rev. B **81**, 041307 (2010).
[18] H.-Z. Lu *et al.*, Phys. Rev. B **81**, 115407 (2010).
[19] D. Teweldebrhan *et al.*, Nano Lett. **10**, 1209 (2010).
[20] Y.-Y. Li *et al.*, arXiv:0912.5054.
[21] G. Mahan and J. Sofo, Proc. Natl. Acad. Sci. U.S.A. **93**, 7436 (1996).
[22] G. Nolas *et al.*, *Thermoelectrics: Basic Principles and New Materials Developments* (Springer, New York, 2001).
[23] M. Lee *et al.*, Nature Mater. **5**, 537 (2006).
[24] D.-Y. Chung *et al.*, Science **287**, 1024 (2000).
[25] H. Kaibe *et al.*, J. Phys. Chem. Solids **50**, 945 (1989).
[26] J. C. Tedenac *et al.*, in *Proceedings of the Symposium on Thermoelectric Materials 1998—The Next Generation Materials for Small-Scale Refrigeration and Power Generation Applications* (Materials Research Society, Boston, 1998), p. 93.
[27] R. Takahashi and S. Murakami, Phys. Rev. B **81**, 161302 (R) (2010).
[28] P. Lee and T. V. Ramakrishnan, Rev. Mod. Phys. **57**, 287 (1985).
[29] R. P. Feynman and Q. R. Hibbs, *Quantum Mechanics and Path Integrals* (McGraw-Hill, New York, 1965).
[30] D. Y. Sharvin and Y. V. Sharvin, JETP **34**, 272 (1981).
[31] T. Ando *et al.*, J. Phys. Soc. Jpn. **67**, 2857 (1998).